JGR Atmospheres

RESEARCH ARTICLE
10.1029/2019JD030648

Diagnosing Observed Stratospheric Water Vapor Relationships to the Cold Point Tropical Tropopause

William Randel[1] **and Mijeong Park**[1]

[1]National Center for Atmospheric Research, Boulder, CO, USA

Key Points:
- Strong correlations between observed stratospheric H_2O and tropical tropopause temperatures trace the stratospheric transport circulation
- Stratospheric H_2O reconstructed from tropopause temperatures explains most of the observed global variability over 1993–2017
- Results preclude a large impact on stratospheric H_2O from convective injection bypassing the tropical tropopause cold trap

Correspondence to:
W. Randel,
randel@ucar.edu

Citation:
Randel, W., & Park, M. (2019). Diagnosing observed stratospheric water vapor relationships to the cold point tropical tropopause. *Journal of Geophysical Research: Atmospheres*, *124*. https://doi.org/10.1029/2019JD030648

Received 15 MAR 2019
Accepted 18 JUN 2019
Accepted article online 26 JUN 2019

Author Contributions:
Conceptualization: William Randel
Methodology: William Randel, Mijeong Park
Writing - original draft: William Randel
Writing – review & editing: Mijeong Park

Abstract Dehydration at the tropical cold point tropopause primarily controls the entry value of water vapor to the stratosphere, with additional (uncertain) contributions from subtropical monsoonal circulations and extreme deep convection. Here we quantify the links of observed stratospheric water vapor with near-equatorial cold point temperature (T_{CP}), based on interannual variations of monthly zonal averages over the period 1993–2017. Water vapor observations are from combined Halogen Occultation Experiment and Aura Microwave Limb Sounder satellite measurements, and cold point temperatures are from high quality radiosondes and GPS satellite data. Interannual water vapor anomalies are highly correlated with T_{CP}, and coherent patterns can be traced in space and time away from the tropical tropopause to quantify transport in the Brewer-Dobson circulation, including diagnosing seasonal changes in circulation. Lagged regressions with T_{CP} are used to reconstruct water vapor variations directly tied to the cold point, and these reconstructions account for a majority of the observed interannual water vapor variability in the lower to middle stratosphere over most of the globe. Small systematic differences from observed water vapor can identify processes not tied to zonal average T_{CP}, and/or possible uncertainties in the satellite measurements.

Plain Language Summary Stratospheric water vapor is controlled by the freeze-drying of air entering the stratosphere across the cold tropical tropopause, in addition to uncertain contributions from extreme deep convection and other processes. This work quantifies how interannual variations in water vapor measured by satellites during 1993–2017 are related to observed fluctuations in tropical tropopause temperature. We demonstrate strong correlations from the observations and use the evolution of correlation patterns to trace the transport of water vapor anomalies throughout the global stratosphere. We use the relationship with observed tropopause temperatures to estimate water vapor changes over time, and these calculations show excellent agreement with the satellite measurements over the entire globe. Our results demonstrate that tropopause temperatures exert a dominant control over global stratospheric water vapor.

1. Introduction

Stratospheric water vapor is primarily controlled by the freeze-drying of air passing the cold point tropical tropopause, under influence of the mean upward tropical Brewer-Dobson circulation. This relationship was proposed by Brewer (1949) to explain the exceptional dryness of the global stratosphere, linked to the extremely cold tropical tropopause. This relationship is now well known, as is obvious in the large seasonal variation of water vapor tied to the annual cycle in tropical tropopause temperatures, that is, the "tape recorder" (Mote et al., 1996). Observations show that the annual cycle in water vapor originates near the cold point tropical tropopause and propagates both vertically in the tropics and quasi-horizontally in the lower stratosphere to cover most of the globe (e.g., Mote et al., 1996; Randel et al., 2001; Rosenlof et al., 1997). We note that this behavior refers to the so-called "entry value" of stratospheric water vapor (H_2O_{entry}), which dominates variability below the middle stratosphere. Water vapor increases with height in the stratosphere due to the slow oxidation of methane (e.g., Randel et al., 1998; Remsberg et al., 1996), and this contribution becomes relatively important above ~25 km, or at higher latitudes where stratospheric air is relatively "aged" (Waugh & Hall, 2002). Beyond the annual cycle, observations have also shown a close link between interannual changes in water vapor and tropical cold point temperature (hereafter T_{CP};), for example, Randel et al. (2004), Fujiwara et al. (2010), Liang et al. (2011), Fueglistaler et al. (2013), Kawatani et al. (2014), and Tweedy et al. (2017). The coupling of H_2O_{entry} with T_{CP} is furthermore confirmed by realistic simulations of water vapor using chemical transport models or Lagrangian trajectory

calculations, where seasonal and interannual variations in imposed T_{CP} are reflected in water vapor behavior (Avery et al., 2017; Fueglistaler et al., 2005; Fueglistaler & Haynes, 2005; Hegglin et al., 2014; Poshyvailo et al., 2018; Schiller et al., 2009; Schoeberl & Dessler, 2011; Schoeberl et al., 2012; Tao et al., 2015; Schoeberl et al., 2018; Wang et al., 2015). Coupling of T_{CP} and stratospheric water vapor on interannual time scales was also highlighted in the modeling studies of Giorgetta and Bengston (1999) and Geller et al. (2002).

While the cold point tropopause exerts a dominant influence on H_2O_{entry}, other potential mechanisms can also contribute. These include the influence of extreme overshooting convection as a mechanism to hydrate the lower stratosphere (e.g., Avery et al., 2017; Corti et al., 2008; Dessler et al., 2007; Hanisco et al., 2007; Khaykin et al., 2009; Sun & Huang, 2015). Small-scale waves and microphysical processes also likely influence the detailed behavior of water vapor near the tropical tropopause (e.g., Fueglistaler et al., 2013; Jensen & Pfister, 2004; Schoeberl et al., 2016; Ueyama et al., 2015, 2018). Improved understanding of the large-scale variability in water vapor directly related to T_{CP} may help identify systematic influences of these additional processes.

The objective of this work is an empirical, quantitative analysis of links between observed interannual variations in stratospheric water vapor and observed T_{CP}, using over 20 years of high quality satellite observations. We use water vapor measurements from the Halogen Occultation Experiment (HALOE; Russell et al., 1993) and Aura Microwave Limb Sounder (MLS; Read et al., 2007), and T_{CP} derived from high quality radiosondes and GPS radio occultation data. For simplicity, we focus on zonal mean behavior and examine deseasonalized, monthly mean anomalies in both quantities. While the respective background seasonal cycles in both quantities exhibit well-known behavior, analyses of interannual variations allow the use of simple lag correlations and regressions to quantify time-varying relationships. We focus on two aspects, discussed in-turn below:

1. How are observed water vapor anomalies related to T_{CP}, and how do the correlated patterns evolve in space and time and with respect to season (reflecting the variable transport circulation in the lower stratosphere)?
2. How much of the interannual variability in water vapor can be captured by optimal correlations with T_{CP}, and what is the behavior of the "residual" variance (not explained by T_{CP})?

2. Data and Analyses

2.1. HALOE and MLS Satellite Water Vapor

We use monthly and zonally averaged water vapor mixing ratio from the HALOE (Russell et al., 1993), covering October 1991 to November 2005 (using retrieval version v19). HALOE is based on solar occultation measurements that have high vertical resolution (~2 km) but limited spatial sampling, requiring approximately 1 month to sample the region 60°N to 60°S. Data are available on standard pressure levels (12 levels per decade of pressure), with the lower level of data at 100 hPa. HALOE data quality is discussed in Kley et al. (2000). As noted in Davis et al. (2016), the HALOE data in 1992 had biases related to Mount Pinatubo volcanic aerosols, and our analyses only use data beginning in January 1993. After construction of monthly zonal mean data over 1993–2005, the HALOE data are deseasonalized with respect to the average monthly seasonal cycle calculated from the entire period.

Water vapor measurements from the Aura MLS (Read et al., 2007) are analyzed for the period September 2004 to December 2017. We utilize MLS retrieval version 4.2 (Livesey et al., 2018). MLS provides much denser space-time sampling than HALOE, with near-global coverage on a daily basis. Data are available for standard pressure levels (12 per decade) for levels 316 to above 1 hPa; the vertical resolution is near 3 km. Data quality for MLS v4.2 are discussed in Hurst et al. (2016) and Livesey et al. (2018). We note that MLS data have somewhat higher uncertainties in the upper troposphere-lower stratosphere region compared to levels near 20 km, and Hurst et al. (2016) suggest a possible slow drift in MLS compared to long-term balloon measurements. Monthly and zonal average MLS data are calculated and deseasonalized with respect to the long-term monthly seasonal cycle.

For longer-term analysis (1993–2017), we generate a combined HALOE + MLS data set by merging the respective deseasonalized HALOE and MLS data records. Merging deseasonalized anomalies from the two

data sets minimizes discontinuities and biases between the data that are inherent in the very different HALOE and MLS satellite measurements. We perform the merging in a simple manner by adjusting the anomalies to match during the overlap period September 2004 to November 2005. Details of this merging are discussed in Randel (2010).

2.2. T_{CP} From Radiosondes and GPS

We derive estimates of monthly average T_{CP} from radiosondes (1993–2017) and GPS radio occultation (2001–2017). The radiosonde results are from an average of three near-equatorial stations with high quality continuous measurements: Nairobi (1°S, 37°E), Manaus (3°S, 60°W), and Majuro (7°N, 171°E). These time series are updated from the data discussed in Randel (2010). For data from Majuro, we use only nighttime measurements after 2011, because of biases in daytime data introduced by a change in radiosonde instruments. Monthly means are simply calculated as the average of the daily cold point, and time series are deseasonalized with respect to the long-term monthly seasonal cycle.

GPS radio occultation provides high vertical resolution temperature profiles spanning late 2001 to present, and we utilize all data within 10°N to 10°S for calculating monthly and zonal averages. The available sampling provides ~500 observations per month prior to 2006 and ~5,000 observations per month after 2006 (following the launch of COSMIC; Anthes et al., 2008). Monthly mean T_{CP} is calculated by averaging the individual profile T_{CP} and hence is based on the full variability of local wave structures (Kim & Alexander, 2015), although we note that nearly identical monthly anomaly time series are obtained if the temperature profiles are first averaged and then T_{CP} calculated. The monthtly average T_{CP} data are deseasonalized by using the respective monthly annual cycle. In general, there is excellent agreement between the T_{CP} anomalies derived from radiosondes and GPS data, as shown below.

3. Results

The background motivation for this work comes from the observed strong correlation between interannual anomalies in near-global (60°N-S) water vapor in the lower stratosphere (83 hPa, near 17.5 km) and corresponding variations in near-equatorial cold point tropopause temperatures (T_{CP}). This is illustrated in Figure 1, which provides an update to similar results published in Randel and Jensen (2013) and Tweedy et al. (2017). The water vapor anomaly time series in Figure 1 (for the 83-hPa level) is from the merged HALOE and MLS data discussed above. Deseasonalized T_{CP} time series in Figure 1 are shown as derived from radiosonde measurements (1993–2017) and a shorter record from GPS (2001–2017). Figure 1 shows excellent agreement between the GPS and radiosonde T_{CP} anomalies over 2001–2017, which enhances confidence in the longer-term radiosonde data. The excellent agreement is due to the fact that much of the low-frequency interannual variability in near-equatorial temperatures occurs with zonally symmetric structure (confirmed by analysis of the latitude-longitude dependent GPS data record; results not shown here) and hence is captured by the three widely spaced radiosonde stations.

Figure 1 demonstrates strong correlations between interannual changes in T_{CP} and lower stratospheric water vapor, with a correlation coefficient of ~0.8 during 1993–2017 (with global water vapor lagging T_{CP} by approximately 2 months). Randel and Jensen (2013) showed that these correlations depend on season, with stronger coherence during boreal winter. Our objective here is to further describe these relationships, including the space-time structure of water vapor correlations as a function of latitude, altitude, and time lag, and changes in correlations with season. Unless otherwise stated, the results presented here focus on the time period 2005–2017 covered by the dense MLS and GPS data records. Some corresponding results for the longer record from HALOE + MLS and radiosondes (1993–2017) are also included.

3.1. Interannual Correlations of Water Vapor With Respect to T_{CP}

Calculations below are based on interannual variations in water vapor and T_{CP}, and several aspects of these data are shown in Figure 2. Figure 2a shows overlain time series of monthly mean T_{CP} for individual years 2005–2017 based on GPS data, highlighting the repeatable annual cycle (cold during boreal winter) together with relatively large interannual variability during the cold months. This variability is driven by fluctuations in dynamical forcing of mean upwelling in the tropopause region (e.g., Abalos et al., 2012); both the mean upwelling and its variability is larger during boreal winter. Figure 2a also shows the altitude and pressure of the cold point tropopause, which is ~0.7 km higher during the cold season (boreal winter).

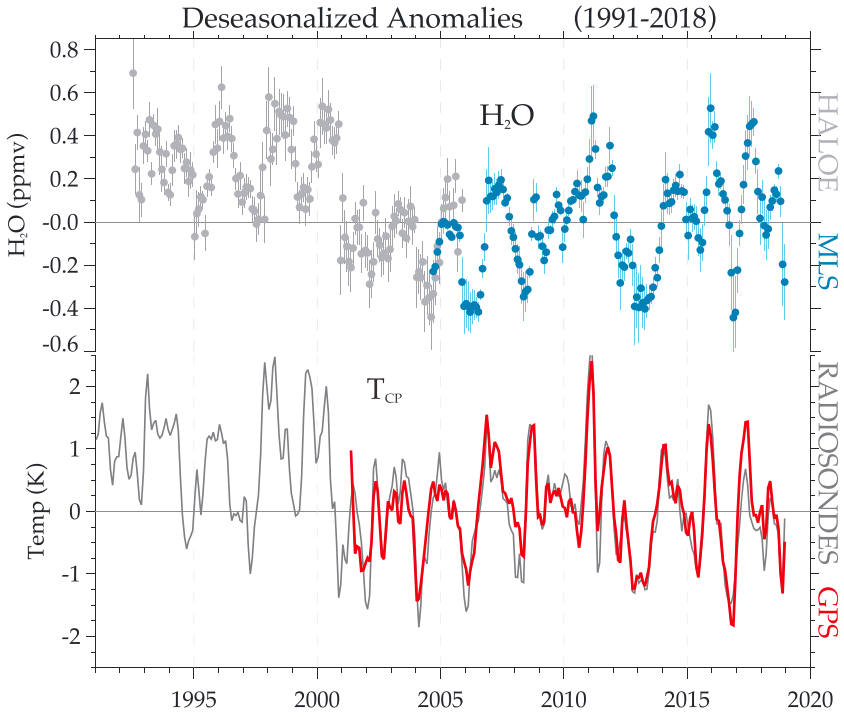

Figure 1. (top) Time series of monthly anomalies in near-global (60°N-S) water vapor in the lower stratosphere (83 hPa) from merged HALOE and MLS data. Monthly means and standard deviations are noted by circles and error bars. (bottom) Temperature anomalies at the tropical cold point tropopause (T_{CP}), derived from radiosondes and GPS satellite data. HALOE = Halogen Occultation Experiment; MLS = Microwave Limb Sounder.

Interannual variability of MLS water vapor as a function of month and latitude is shown in Figure 2b for pressure levels 100, 83, and 68 hPa, calculated simply as the variance for each individual month over 2005–2017. The largest variability occurs centered on the equator for the 83-hPa level during boreal winter (~November–April), approximately following the enhanced T_{CP} variability for these months seen in Figure 2 a; note that the cold point pressure is near 85–90 hPa in these months. Interannual variability in water vapor at 100 hPa is smaller than at 83 hPa, with weak maxima during October-November and May-June during the tropopause transition seasons. Water vapor variations at 68 hPa maximize later in boreal winter compared to 83 hPa, and this time lag reflects upward propagation of anomalies described below. There is a separate maximum during August-September at 68 hPa situated slightly north of the equator, which may reflect variations tied to the boreal summer monsoons. The key results here highlight larger T_{CP} and water vapor variability during boreal winter, and we separate results below based on the seasonality in Figure 2.

We evaluate the correlations between T_{CP} and water vapor as a function of latitude, height, and time lag in order to trace patterns of coherent variability linked to transport of water vapor anomalies from their origin near the cold point tropopause. In order to study seasonally evolving patterns, we separate the calculations based on individual months; that is, T_{CP} anomalies in January are correlated with water vapor anomalies in January and subsequent months. Contemporaneous correlations (lag = 0) for January and June are shown in Figure 3. The cold point tropopause is near 17.3 km in January (Figure 3a), and the strongest correlations with water vapor (>0.9) are found in the tropics (~30°N-S) centered near the 83-hPa level. In June (Figure 3b), the cold point tropopause is near 16.6 km, and strongest water vapor correlations (>0.85) occur at a corresponding higher pressure centered at 100 hPa.

A scatter plot of water vapor at 83 hPa (near the cold point) versus T_{CP} anomalies in January is shown in Figure 4, highlighting the strong correlation. Figure 4 includes water vapor and T_{CP} statistics based on the MLS and GPS data records (2005–2017) and also covering the extended period 1993–2017 using merged HALOE + MLS and radiosonde data. The slope of the ($\Delta H_2O/\Delta T$) regression in Figure 4 is approximately consistent with the slope expected from the Clausius-Clapeyron relationship (at relative humidity over ice = 100%) evaluated near the tropical tropopause (T_{CP} ~ 190 K, pressure ~ 90 hPa), which is ~0.5 ppmv/K

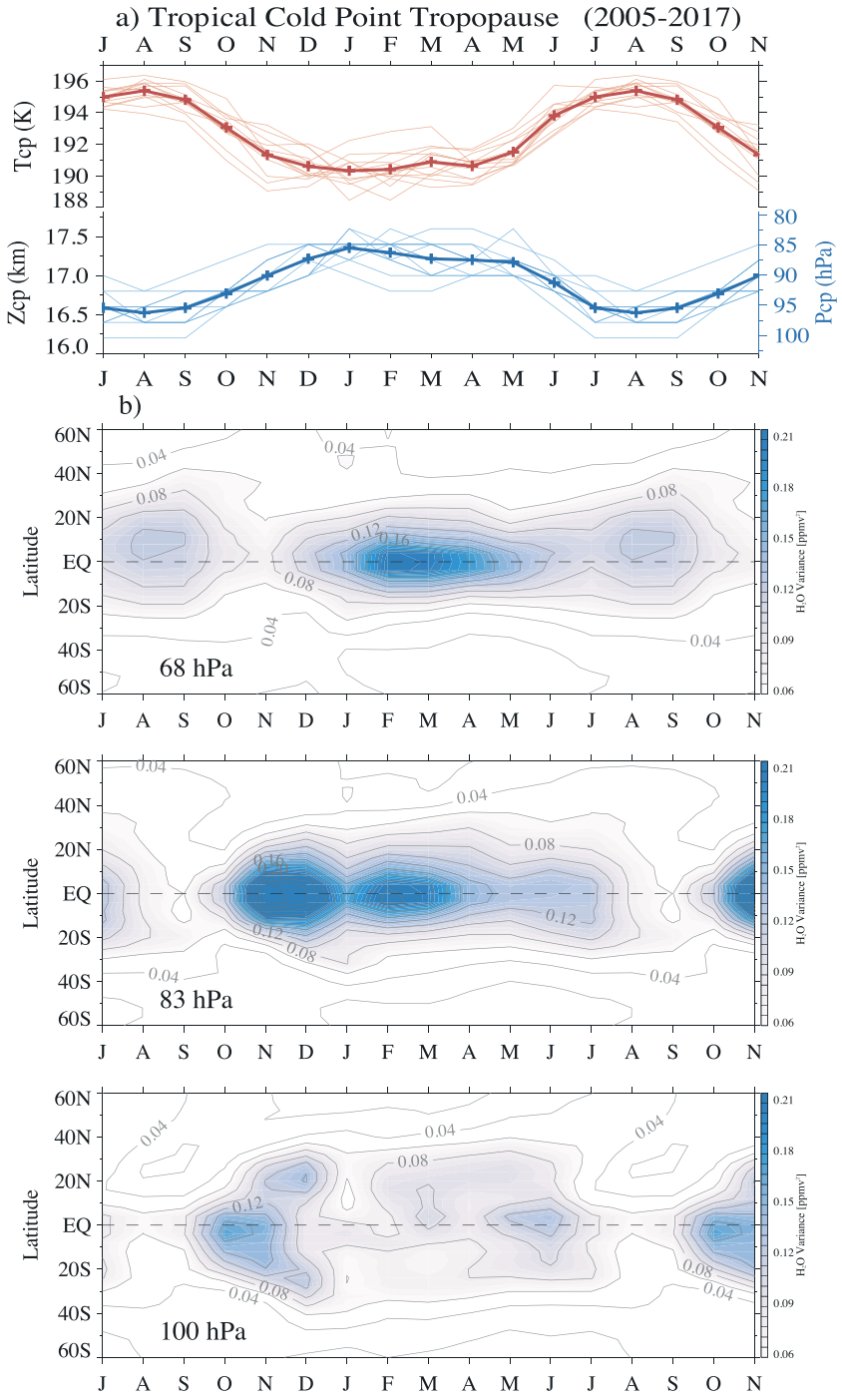

Figure 2. (a) Time series of monthly average tropical cold point tropopause temperature (T_{CP}) and altitude/pressure. Data are from GPS radio occultation measurements over 10°N-S, and the heavy curves show the long-term means. (b) Interannual variance in water vapor as a function of latitude and month for the 100-, 83-, and 68-hPa levels, derived from MLS data over 2005–2017. Note the time axis partially repeats, covering July–November.

(e.g., Fueglistaler & Haynes, 2005). Thus, although the HALOE and MLS water vapor retrievals represent ~2- to 3-km-thick vertical layer averages, interannual anomalies near the tropical tropopause are in quantitative agreement with expectations from the observed T_{CP} anomalies.

As time lags progress, maximum water vapor correlations extend away from the tropical tropopause region, with the patterns rising in altitude and spreading in latitude following the stratospheric Brewer-Dobson

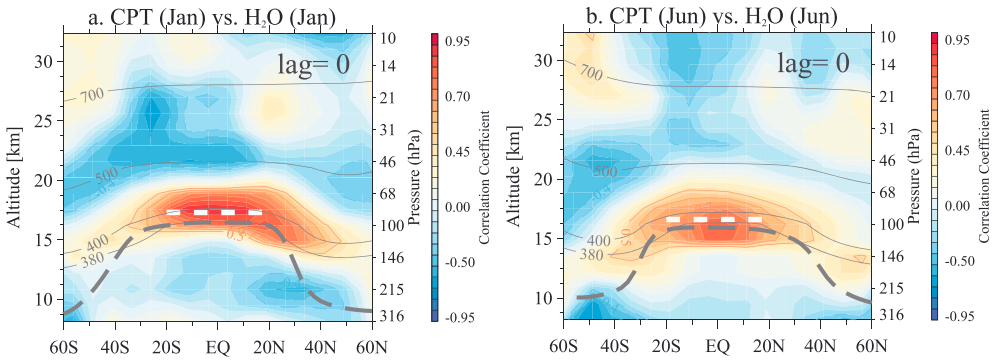

Figure 3. Contemporaneous correlation of interannual anomalies in water vapor mixing ratio at each latitude and height versus tropical cold point temperature (T_{CP}), derived from Microwave Limb Sounder H_2O and GPS T_{CP} statistics in January (a) and June (b). The gray dashed line indicates the average lapse rate tropopause, the white dotted line is the cold point tropopause, and the solid black lines are isentropes. CPT = cold point temperature.

circulation. Figure 5 shows water vapor correlations with T_{CP} at lags of 2, 4, 8, and 10 months, with respect to T_{CP} in January and June; these patterns trace the transport of zonal average water vapor anomalies away from the tropical tropopause in the boreal winter and summer seasons. In January, at a lag of 2 months, the correlations have risen slightly in altitude and spread in latitude to cover most of the globe in the lower stratosphere. The slope of the strongest correlations approximately follow the sloping isentropic levels ~400 K in the lower stratosphere, and this reflects rapid quasi-horizontal transport of water vapor anomalies from the tropics to higher latitudes. The deep tropical correlations (~20°N-S) trace upward movement of the anomalies with increasing time lag, with strongest values centered near ~37 hPa (~22 km) after 10 months.

Lag correlation patterns with respect to June T_{CP} in Figure 5 show horizontal spreading of lower stratosphere correlations mainly toward the Southern Hemisphere, with strong correlations filling the extratropical lowermost stratosphere after several months. The lack of stronger correlations extending into the Northern Hemisphere (NH) might possibly reflect influence of the boreal summer monsoons on lower stratospheric water vapor; behavior in the monsoon regions may be more influenced by regional temperatures (Randel et al., 2015) and have less correlation with near-equatorial zonal mean T_{CP}. This influence of the monsoon regions on lower stratosphere water vapor can be viewed clearly in monthly average MLS data, as shown in the evolution during August–October 2017 in Figure 6. This reflects the contribution of the monsoon regions to the "moist phase" of the tape recorder signal, as has been inferred in modeling studies of water vapor, for example, Gettelman et al. (2004), Poshyvailo et al. (2018), and Nützel et al. (2019). While it is difficult to quantify the contributions from monsoon versus the freeze-drying of air masses ascending across the tropical tropopause from observations, this process undoubtedly contributes to the weaker NH correlations following boreal summer seen in Figure 5.

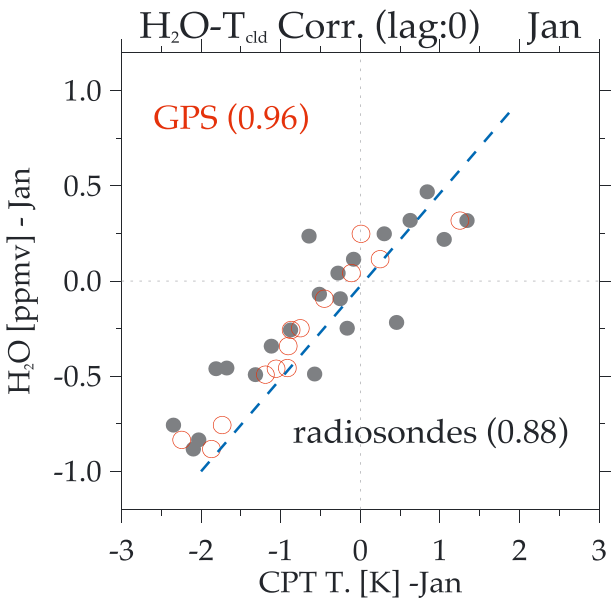

Figure 4. Scatter plot of interannual anomalies in water vapor (at 83 hPa, 10°N-S) versus T_{CP}, for data in January. Red points are for the MLS-GPS record (2005–2017), and gray points for the HALOE + MLS and radiosonde data (1993–2017). The dashed line shows the ($\Delta H_2O/\Delta T_{CP}$) slope expected from the Clausius-Clapeyron relationship at this location (~0.5 ppmv/K), as explained in the text. MLS = Microwave Limb Sounder; HALOE = Halogen Occultation Experiment; CPT = cold point temperature.

In Figure 5 the tropical correlations with respect to T_{CP} in June propagate upward, with maxima centered south of the equator. The tropical correlations above ~20 km relative to June are somewhat weaker compared to those for January, which could reflect influence of the boreal monsoons noted above, and/or the fact that T_{CP} and tropopause-level water vapor anomalies are somewhat smaller during boreal summer (Figure 2b). Regardless of the magnitude, it is interesting to note that the net upward displacement of the tropical January and June patterns are similar at time lags of 8–10 months (i.e., near 22 km after lag of 10 months), in spite of the well-known approximately factor of 2 difference in tropical upwelling

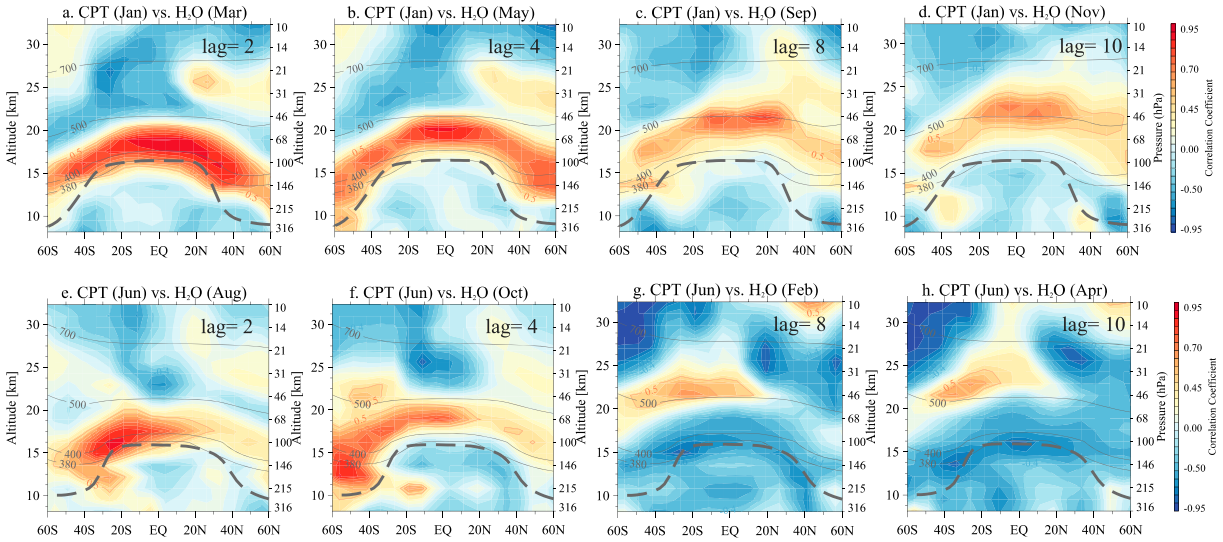

Figure 5. Correlations of water vapor anomalies at each latitude and height versus T_{CP} as a function of time lag (2 to 10 months, left to right), showing statistics referenced in January (a–d) and June (e–h). Details are the same as in Figure 3. CPT = cold point temperature.

strength between these seasons (stronger in boreal winter; e.g., Abalos et al., 2015). This may be explained by the fact that water vapor anomalies experience the full annual cycle in upwelling velocity while transiting from the tropopause to above 20 km over ~12 months.

The coherent vertical propagation of tropical water vapor anomalies are quantified by tracing the water vapor correlations with T_{CP} in time, as shown in Figure 7. Patterns originating in January (Figure 7a) can be traced continuously for more than 18 months to altitudes above 30 km. The overall net upward speed of the anomalies is near ~8 km/year, consistent with previous estimates of average tropical upwelling derived from water vapor in Niwano et al. (2003), Schoeberl et al. (2008), and Glanville and Birner (2017). Closer inspection shows that the slope of the correlations changes over the annual cycle, with faster upward movement during boreal winter (black dashed lines in Figure 7a), and this is consistent with seasonal variations in tropical upwelling. The correlation patterns beginning in June (Figure 7b), which originate a little lower because of the lower altitude tropopause, do not extend as high into the stratosphere as those for January, although the net upward speed is still near 8 km/year.

3.2. Reconstructing Stratospheric Water Vapor From Observed T_{CP}

The objective of this section is to quantify the influence of T_{CP} on global stratospheric water vapor. We reconstruct monthly time series of water vapor anomalies at each latitude and height using regressions onto T_{CP} with optimal time lags and then compare with actual observed water vapor anomalies. The differences

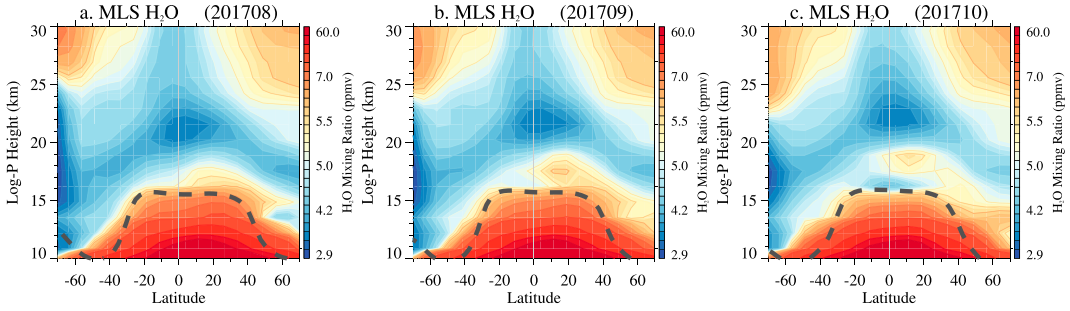

Figure 6. Zonal average MLS water vapor measurements from (a) August, (b) September, and (c) October 2017. The evolving maxima in the Northern Hemisphere lower stratosphere show influence of the boreal summer monsoons. MLS = Microwave Limb Sounder.

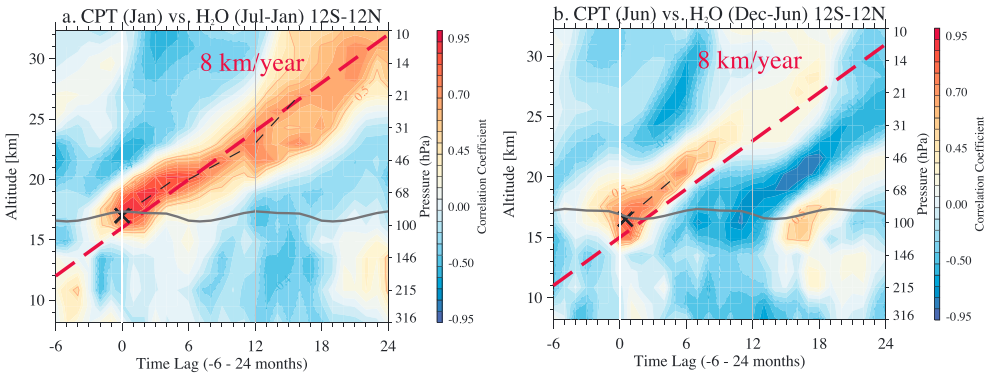

Figure 7. Altitude versus time patterns of water vapor correlation with T_{CP} over the equator, for statistics originating in January (a) and June (b). The dashed white line is the cold point tropopause. The black dashed lines trace the maximum correlations upward from the tropopause, and the dashed red lines indicate an upward speed of 8 km/year. CPT = cold point temperature.

or residuals then provide an estimate of the importance of processes not directly related to zonal average T_{CP} for stratospheric water vapor.

The reconstructions are performed as follows. For each month of the year, we calculate the correlation between water vapor (at each latitude and pressure level) and T_{CP} as a function of time lag, and choose the time lag (τ) with the highest correlation. For example, for water vapor in May at 0° and 56 hPa, the optimal time lag is 4 months (see Figure 5). We then calculate reconstructed water vapor anomalies (H_2O_{recon} (ϕ, p, t)) using the following:

$$H_2O_{recon}\ (\phi, p, t) = (\Delta H_2O/\Delta T_{CP})^* T_{CP}\ (t-\tau). \quad (1)$$

Here ($\Delta H_2O/\Delta T_{CP}$) is the slope estimated by regression between water vapor and (optimally lagged) T_{CP}, such as that shown in Figure 4. This procedure is repeated for each latitude, pressure, and month, and results are combined to generate full time series of water vapor anomalies that are optimally fit to T_{CP}. The patterns of derived time lag τ and slope ($\Delta H_2O/\Delta T_{CP}$) are generally coherent in the latitude-height plane, with τ increasing away from the tropical tropopause region and the slope decreasing (results not shown here). Figure 8 shows results of this reconstruction over the equator at 83 and 56 hPa, compared with the actual

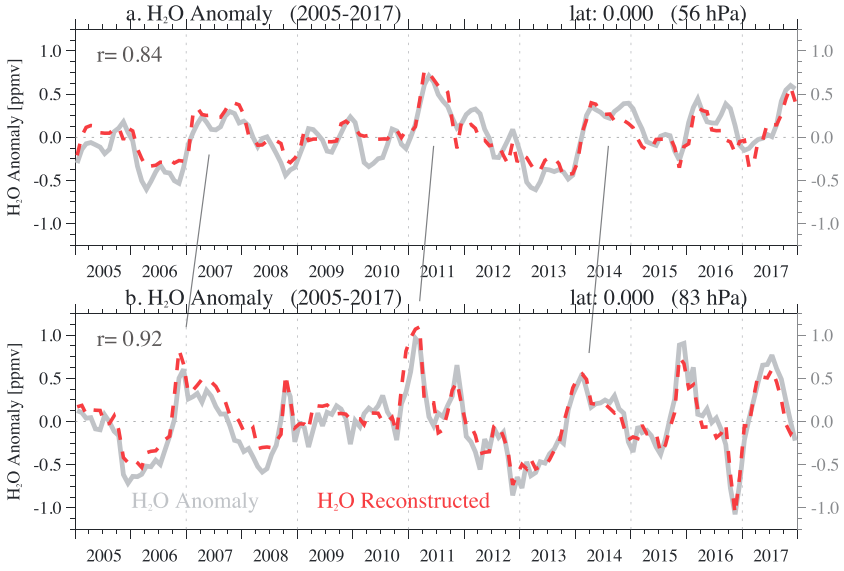

Figure 8. Time series of water vapor anomalies at the equator for (a) 56 and (b) 83 hPa. Gray lines are observed anomalies, and red dashed curves show water vapor anomalies reconstructed from T_{CP}.

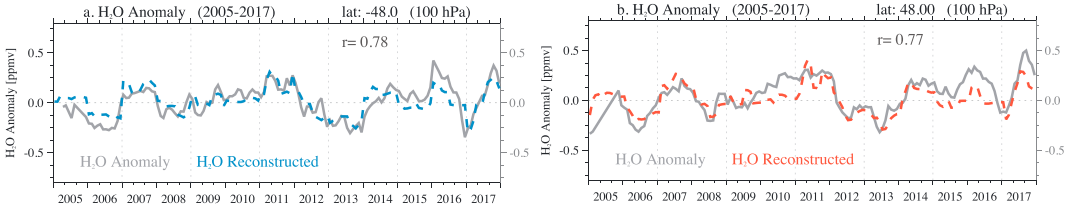

Figure 9. Time series of observed (gray) and reconstructed (blue/red) water vapor anomalies in the extratropical lower stratosphere, for 100 hPa data at 48°S (a) and 48°N (b).

observed water vapor anomalies. Results show strong correlations between observed and reconstructed water vapor: 0.92 at 83 hPa and 0.84 at 56 hPa. Figure 8 shows that these calculations capture both the time lag and amplitude decrease for water vapor anomalies propagating upward in the tropics. The amplitude decrease is a result of mixing of the anomalies during vertical propagation (e.g., Mote et al., 1998), and this effect is captured in the regressions through a change in the ($\Delta H_2O/\Delta T_{CP}$) slope at each location. We find similar behavior for propagation in latitude, as shown for the time series at 100 hPa, 48°N and 48°S in Figure 9. Note the similarity of the water vapor anomalies in extratropics of both hemispheres in Figure 9, due to propagation from the tropical source region in both cases.

Time series of water vapor reconstructed from T_{CP} capture much of the interannual variance throughout the lower stratosphere. Figure 10a shows the correlation between reconstructed and observed water vapor as a function of latitude and altitude for the MLS-GPS data record, revealing high correlations (>0.7) throughout the lower stratosphere over most of the globe (~60°S to 90°N), and extending upward in the tropics to the middle stratosphere. Weaker correlations in the Antarctic are probably related to the strong polar vortex and in situ dehydration in this region during austral winter-spring, which decouples water vapor variability from lower latitudes. The correlations in the tropics above 46 hPa (~22 km) in Figure 10a are somewhat weaker than below, and this reflects additional variations in water vapor possibly linked to CH_4 oxidation and fluctuations in tropical upwelling, as discussed below. The strong correlations in Figure 10a mimic the patterns of water vapor anomaly evolution seen in Figure 5, that is, transport of near-equatorial anomalies to high latitudes of both hemispheres in the lower stratosphere and upward in the deep tropics. Correlations are relatively low in extratropics above ~20 km, presumably because a larger fraction of the extratropical H_2O at these altitudes has come from CH_4 oxidation and/or the mixing of descending polar air (cf. Figure 6). There is relatively small interannual variability of water vapor in these regions. A map of the interannual variance in water vapor is shown in Figure 10b, revealing relatively large values in the tropics and in the extratropical lower stratosphere of both hemispheres close to the tropopause. Most of the variance in the tropics and in the extratropics for pressures below ~146 hPa is explained by T_{CP} (Figure 10a).

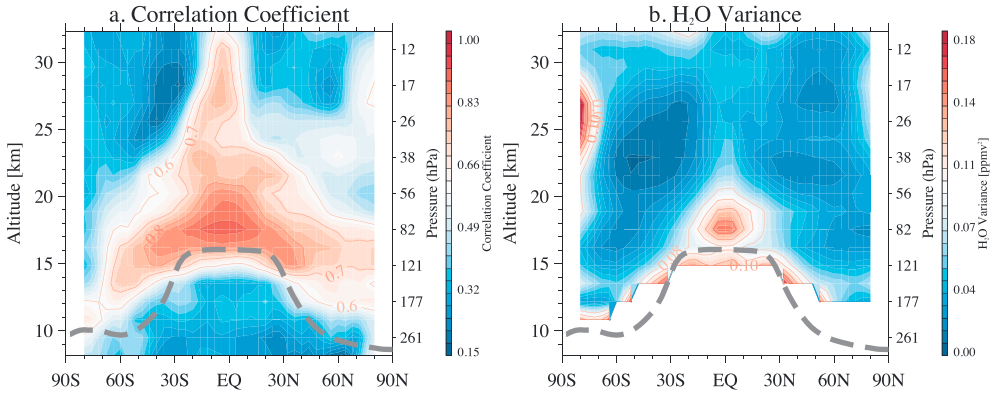

Figure 10. (a) Correlation between observed Microwave Limb Sounder water vapor anomalies and time series reconstructed from T_{CP}, for data over 2005–2017. (b) Interannual variance in water vapor (ppmv^2). Note that these plots cover 80°N-S.

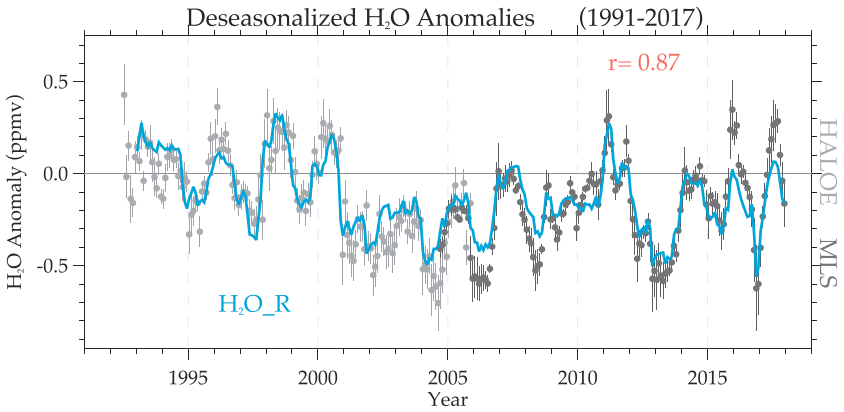

Figure 11. Time series of observed near-global (60°N-S) stratospheric water vapor at 83 hPa (as in Figure 1), together with values reconstructed from T_{CP} (blue line). HALOE = Halogen Occultation Experiment; MLS = Microwave Limb Sounder.

We performed similar calculations for the extended HALOE + MLS satellite data record. These calculations were based on equation (1), using ($\Delta H_2O/\Delta T_{CP}$) evaluated from the MLS-GPS period (with dense data coverage), and T_{CP} over 1993–2017 derived from merging radiosonde data before 2001 with GPS data afterward. Figure 11 shows time series of near-global (60°N-S) H_2O at 83 hPa derived from this reconstruction together with the observed data (from Figure 1), showing that the reconstruction tracks most of the detailed interannual changes over the full 25-year data record (including the well-known "drop" in 2000), with an overall correlation of $r = 0.87$. The differences between the satellite measurements and reconstructed H_2O in Figure 11 are larger near the end of the data record (>2015), and these could reflect possible biases in the MLS data record, as discussed below. In spite of these differences, the overall agreement in Figure 11 demonstrates the strong control of T_{CP} on lower stratosphere water vapor for the 25-year record of high quality satellite measurements.

3.3. Residual Water Vapor Variance in the MLS-GPS Data Record

The results in Figures 8–10 show that most of the interannual variability in stratospheric water vapor in the MLS data record is related to T_{CP} in a relatively simple manner, namely, the propagation of anomalies originating near the cold point tropical tropopause. As discussed further below, the actual transport is certainly more complex and involves a range of transport times (as quantified by a stratospheric age-of-air or transit-time spectrum; e.g., Waugh & Hall, 2002), but the simple calculations here in fact explain large fractions of the observed variance. Here we explore behavior of the residual, or difference between observed H_2O and that reconstructed from T_{CP}: $H_2O_{residual} = H_2O_{observed} - H_2O_{recon}$. The residual, or unexplained variance, may contain information on processes influencing H_2O_{entry} that are not tied in a simple manner to T_{CP}, and here we explore this residual for the MLS data record.

Variations in deseasonalized MLS water vapor at 83 hPa as a function of latitude and time are shown in Figure 12a, highlighting interannual anomalies that originate in the deep tropics and propagate to both hemispheres. As shown above, the majority of this variability is tied in a simple manner to T_{CP}. Figure 12 b shows the differences between the observed and reconstructed water vapor (residual) at 83 hPa; for reference, time series of observed and reconstructed water vapor at 83 hPa and 0° are shown in Figure 8a. The residuals can arise from a number of sources: regional (nonzonal) structure in the H_2O-T_{CP} relationships that do not average out in the zonal mean, additional physical processes such as deep overshooting convection, or uncertainties in the satellite H_2O or T_{CP} data. The residuals in Figure 12b are small compared to the full anomalies, with typical variations of 0.1–0.2 ppmv (root-mean-square values of ~0.1 ppmv near the equator), compared to observed variations of up to ±1 ppmv (Figure 8b). The residuals in Figure 12b often show maxima in the tropics that subsequently propagate to higher latitudes (similar to the anomalies themselves in Figure 12a), and this behavior suggests small physical variations in water vapor not captured in the zonal mean T_{CP} regressions. We note that the patterns in Figure 12b do not show large seasonally synchronized patterns, for example, monsoon maxima. Some of the larger episodic residuals in Figure 12b appear related to large La Nina (2007–2008 and 2010–2011) and El Nino (2015–2016) events, with negative and positive

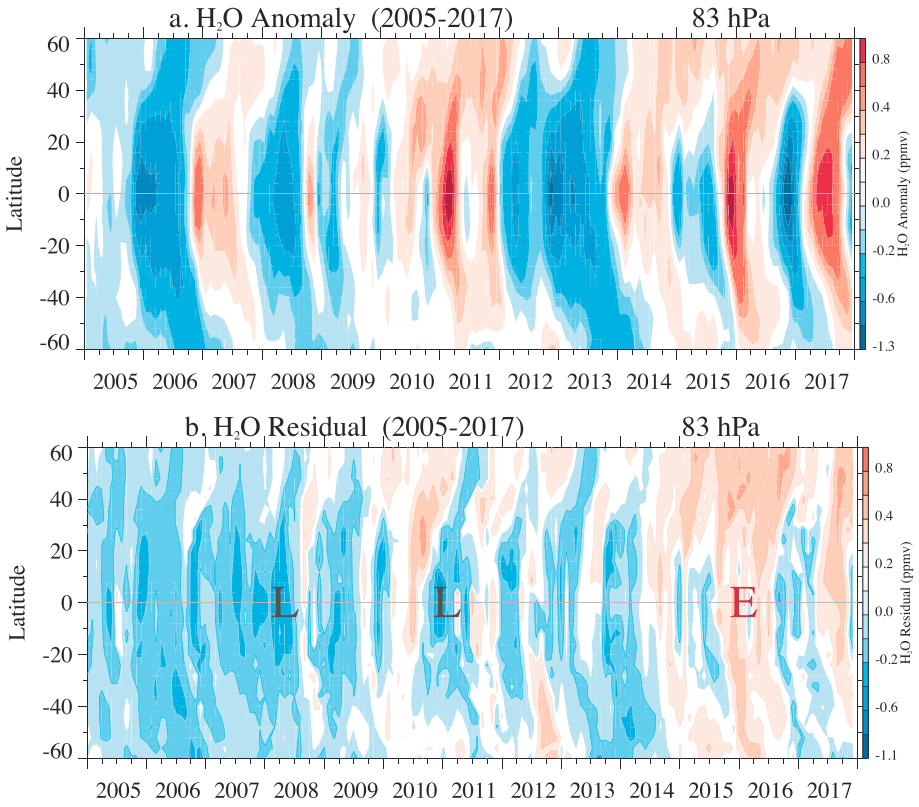

Figure 12. (a) Deseasonalized anomalies of Microwave Limb Sounder water vapor at 83 hPa. (b) Differences between the observed anomalies and time series of water vapor reconstructed from lagged regressions onto T_{CP} ("residuals"). "L" and "E" denote large La Nina and El Nino events during 2005–2017.

tropical H_2O residuals, respectively. Such El Nino–Southern Oscillation (ENSO) events are known to be associated with strong zonal asymmetries in H_2O near the tropical tropopause (Avery et al., 2017; Garfinkel et al., 2018; Konopka et al., 2016), which may be tied to this behavior.

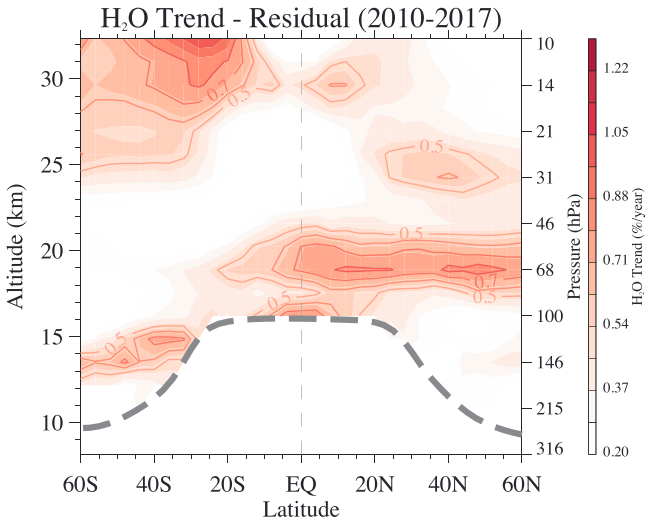

Figure 13. Linear trends in the "residual" stratospheric water vapor over 2010–2017 as a function of latitude and height. Residuals are calculated as observed water vapor minus time series reconstructed from T_{CP}. Units are %/year.

Aside from the episodic ENSO events, the overall patterns of the residuals in Figure 12b show some clear trend-like behavior, with stronger negative residuals at the beginning of the record evolving to positive over 2005–2017, that is, the MLS H_2O data are becoming moister over time compared to time series expected from observed T_{CP}. This trend-like behavior in the residuals could point to actual physical changes, such as the influence of CH_4 oxidation or increasing deep tropical convection, or to systematic changes in the data. Figure 13 shows the structure of linear trends in the H_2O residual to help understand this behavior. Here linear trends are calculated over the period 2010–2017, motivated by MLS comparisons with balloon measurements showing trend-like biases in MLS after 2010 (Hurst et al., 2016). Trends in Figure 13 show a strong maximum in the lower stratosphere (largest over MLS levels ~83–56 hPa), with largest trends in the NH near 0.7–0.9 %/year, which equates to net changes of ~0.2–0.3 ppmv over 2010–2017. The spatial structure in Figure 13 does not seem obviously linked to physical behavior such as CH_4 oxidation, which would have a pattern more similar to stratospheric age of air, or changes in tropical convection, which would maximize in the tropics closer to the tropopause. Rather, these trends may reflect small systematic artificial moistening trends in the MLS H_2O data, as proposed by Hurst et al. (2016). The stronger trends in the NH in Figure 13 are consistent

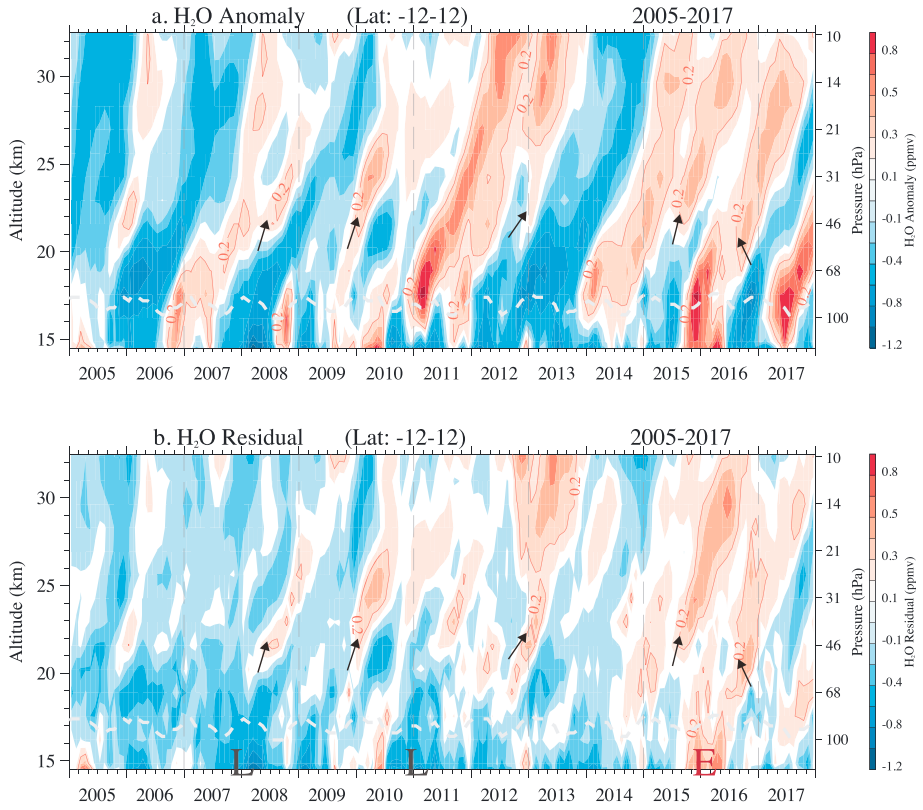

Figure 14. (a) Height versus time section of deseasonalized anomalies of Microwave Limb Sounder water vapor over the equator (12°N-S), that is, the interannual anomaly "tape recorder." (b) Differences between the observed anomalies and time series of water vapor reconstructed from lagged regressions onto T_{CP} ("residuals"). The white dashed line is the cold point tropopause, and the "L" and "E" symbols at the bottom of panel (b) denote large La Nina and El Nino events (as in Figure 12b). Arrows in both panels indicate several H_2O maxima not directly linked to T_{CP}, and hence emphasized in the residuals.

with this hypothesis, as there is additional evidence to suggest the artificial MLS trends are larger in the NH lower stratosphere (Hurst et al., 2016; N. Livesey, personal communication, March 8, 2019). In summary, while the residuals identified in our calculations (Figure 12b) are small, they contain a signature of what seem to be artificial moistening trends in the MLS H_2O data in the lower stratosphere. When this is taken into account, the residuals in our calculations would be substantially smaller.

One further aspect of water vapor variability is identified from our analyses of residuals. Figure 14a shows a height versus time plot of water vapor anomalies near the equator (the tape recorder for interannual anomalies), showing the familiar upward propagation of anomalies originating near the cold point tropopause. These variations are mostly captured by the regressions onto T_{CP}, especially in the lower stratosphere, and hence are associated with relatively small residuals (Figure 14b). However, there are additional variations in water vapor that do not originate near the tropopause but rather at slightly higher altitude (often near ~50 hPa, as indicated by the arrows in Figure 14) and then propagate coherently upward. These variations are not simply correlated to T_{CP} and are isolated in the residuals from the T_{CP} regressions (Figure 14b). The latitudinal structure of these residual variations at 46 hPa shows maxima centered over the equator (~20°N-S; figure not shown), showing that they do not originate in extratropical latitudes, and the variability is not synchronized to the annual cycle, such as might result from boreal monsoon effects. One relatively simple mechanism for these H_2O anomalies originating in the tropics above ~22 km could be variations in near-equatorial upwelling and associated CH_4 oxidation, that is, slower upwelling linked with enhanced CH_4 oxidation and positive H_2O anomalies. This altitude dependence of CH_4 influence above ~22 km is consistent with the simulations of Schoeberl et al. (2012), their Figure 6. We evaluated this hypothesis by comparing residuals in Figure 14b with time series of interannual variations in tropical upwelling (w^*) derived

from reanalysis data, as in Abalos et al. (2015; using updated results provided courtesy of Marta Abalos; results not shown here). The comparisons show approximate qualitative agreement, with positive H_2O residuals in Figure 14b associated with negative w^* anomalies over 50–30 hPa. While these comparisons are consistent with our hypothesis of variations in tropical upwelling and CH_4 oxidation as a source for the residual H_2O anomalies, we leave more detailed analysis for future work. Whatever their origin, the existence of these additional sources of H_2O variability in the deep tropics above ~22 km helps explain the somewhat weaker correlations between observed and reconstructed H_2O above these altitudes in Figure 10a compared to levels closer to the tropopause.

4. Summary and Discussion

This work is aimed at quantifying the well-known relationship between stratospheric water vapor and tropical tropopause T_{CP}, based on interannual changes from a long record of satellite observations. The largest interannual variations in H_2O originate during boreal winter at the 83-hPa level near the equator (Figure 2) and are highly correlated with contemporaneous T_{CP} ($r > 0.9$; Figure 3). Smaller, but highly correlated, interannual variations in H_2O and T_{CP} are found during boreal summer. There is a simple linear relationship between variations in water vapor and T_{CP} ($\Delta H_2O/\Delta T_{CP}$), which closely follows the Clausius-Clapeyron relationship. This behavior is consistent with a simple picture of stratospheric H_2O control by dehydration at the cold point tropopause. Time-lag correlations demonstrate the rapid propagation of the near-equatorial H_2O anomalies to high latitudes in the lower stratosphere, approximately following (sloping) isentropic levels near 400 K, along with upward propagation in the tropics. These are well-known aspects of H_2O transport as seen in satellite observations (Gilford et al., 2016; Mote et al., 1996; Randel et al., 2001; Rosenlof et al., 1997) and model simulations (e.g., Poshyvailo et al., 2018). Our results have quantified the seasonally varying behavior of the H_2O transport and T_{CP} influences: During boreal winter coherent H_2O variations extend to both hemispheres in the lower stratosphere and to altitudes above 30 km in the tropics (Figures 5 and 7). During boreal summer the time-lagged H_2O correlations with T_{CP} are weaker in the tropics and in the NH lower stratosphere, and we interpret this as being a result of additional H_2O variability tied to transport from the boreal summer monsoons (Figure 6), which is less coupled to zonal mean T_{CP}. We note that the global H_2O correlation patterns in Figure 5, including the seasonal behavior, are similar to the simulated transport patterns for idealized pulse tracers shown in Ploeger and Birner (2016, their Figure 2).

We have used the observed strong time-lag correlations between H_2O and T_{CP} to reconstruct H_2O anomalies at each latitude and height, using lagged regressions onto observed T_{CP}. We note that the corresponding slope of ($\Delta H_2O/\Delta T_{CP}$) changes as a function of location, accounting for the reduced amplitude of H_2O anomalies with distance from the tropical tropopause, attributable to large-scale mixing. This simple reconstruction accounts for a high fraction of the interannual variance in H_2O in the global lower stratosphere and in the tropics up to ~30 km, where the observed variability of H_2O is relatively large (Figure 10). These results quantify the controlling influence of near-equatorial tropopause temperatures (T_{CP}) on water vapor in the extratropical lower stratosphere above ~380 K (~13 km; see Figure 10), where water vapor's radiative impact on global climate is strongest (Forster & Shine, 1999; Gilford et al., 2016; Maycock et al., 2013; Solomon et al., 2010). Extratropical upper troposphere-lower stratosphere water vapor changes below ~13 km are less controlled by T_{CP} and may be more closely linked to tropospheric temperatures and circulation, as suggested by the model results of Dessler et al. (2013). Extension of the H_2O reconstruction for the longer 1993–2017 period, using T_{CP} anomalies obtained from radiosonde data, show that variations in observed T_{CP} can explain most of the temporal variability for near-global H_2O in the lower stratosphere for the merged HALOE + MLS data record (Figure 11).

The accurate overall reconstruction of water vapor in the lower stratosphere from T_{CP} prompts analysis of differences from observations (residuals), as possibly identifying additional controlling processes. The residuals in our calculations are small in the lower stratosphere (~10–20% of the actual interannual variability), with root-mean-square values of ~0.1 ppmv (Figure 12b). The residuals often exhibit maxima in low latitudes and could result from a number of causes, such as nonzonal tropical structure (including ENSO effects), influence of extreme convection or monsoonal circulations (not tied to T_{CP}), or uncertainty in the satellite

data. Variability and trends in transport could also influence the residuals, although such changes are expected to be small (a few percent per decade; e.g., Abalos et al., 2015) and would be difficult to untangle in our analyses. The residual patterns in Figure 12b do not exhibit systematic seasonal patterns, for example, monsoon effects. We do find relatively large episodic residuals in the lower stratosphere associated with large ENSO events during 2005–2017.

One pattern that is obvious in the lower stratospheric residuals in Figure 12b is a net positive trend over the MLS record. This represents a systematic moistening of the MLS H_2O data compared to that expected from the (highly accurate) observed T_{CP} from GPS data. The pattern of these trends as a function of latitude and height (Figure 13) shows banded vertical structure in the lower stratosphere (maximum at the 68-hPa level) with larger trends in the NH. This is an unphysical behavior and may be linked to artificial moistening trends in the MLS H_2O retrievals over time, as suggested by Hurst et al. (2016). When these trends are removed, the residual variance in our calculations is even smaller. Such artificial moistening biases in MLS data (net changes of ~0.2–0.3 ppmv in the lower stratosphere) may explain some of the systematic differences between the merged satellite data record and reconstructed H_2O at the end of the data record (>2015) in Figure 11.

Removal of the H_2O variability linked to T_{CP} reveals further details of the observed H_2O evolution in the tropics, including behavior of the iconic tape recorder signal. While almost all of the interannual H_2O variance below ~22 km (46 hPa) is closely tied to T_{CP}, additional maxima occur above this level that do not originate near the tropopause. These maxima have latitudinal patterns centered over the equator and propagate vertically in a coherent manner, suggesting true geophysical structure. The lack of seasonal synchronization suggests they are not linked to summer monsoon influence at lower levels. While these features remain a topic of study, the overall space-time behavior suggests a possible source due to CH_4 oxidation, in response to variations in tropical upwelling (slower upwelling associated with positive H_2O anomalies).

Acknowledgments
The National Center for Atmospheric Research (NCAR) is sponsored by the U.S. National Science Foundation (NSF). This work was partially supported by the NASA GNSS Remote Sensing Science Team under grant NNX16AK37G. The data used in this study were obtained from the following web sites: HALOE H_2O (https://disc.gsfc.nasa.gov/datacollection/UARHA2FN_019.html), MLS H_2O (https://doi.org/10.5067/Aura/MLS/DATA2009), radiosonde temperatures (https://www.ncdc.noaa.gov/data-access/weather-balloon/integrated-global-radiosonde-archive), and GPS temperatures (https://cdaac-www.cosmic.ucar.edu). We thank Marta Abalos for discussions and updated estimates of tropical stratospheric upwelling derived from meteorological reanalyses and Nathaniel Livesey for discussions regarding details of the MLS H_2O data. We also thank Rolando Garcia, Daniel Gilford, Eric Jensen, Mark Schoeberl, and three anonymous reviewers for suggestions and constructive comments on the manuscript.

References

Abalos, M., Legras, B., Ploeger, F., & Randel, W. J. (2015). Evaluating the advective Brewer-Dobson circulation in three reanalyses for the period 1979–2012. *Journal of Geophysical Research: Atmospheres*, *120*, 7534–7554. https://doi.org/10.1002/2015JD023182

Abalos, M., Randel, W. J., & Serrano, E. (2012). Variability in upwelling across the tropical tropopause and correlations with tracers in the lower stratosphere. *Atmospheric Chemistry and Physics*, *12*(23), 11,505–11,517. https://doi.org/10.5194/acp-12-11505-2012

Anthes, R. A., Bernhardt, P. A., Chen, Y., Cucurull, L., Dymond, K. F., Ector, D., et al. (2008). The COSMIC/FORMOSAT-3 mission: Early results. *Bulletin of the American Meteorological Society*, *89*(3), 313–334. https://doi.org/10.1175/BAMS-89-3-313

Avery, M. A., Davis, S. M., Rosenlof, K. H., Ye, H., & Dessler, A. E. (2017). Large anomalies in lower stratospheric water vapour and ice during the 2015–2016 El Niño. *Nature Geoscience*, *10*(6), 405–409. https://doi.org/10.1038/ngeo2961

Brewer, A. W. (1949). Evidence for a world circulation provided by measurements of helium and water vapor distribution in the stratosphere. *Quarterly Journal of the Royal Meteorological Society*, *75*(326), 351–363. https://doi.org/10.1002/qj.49707532603

Corti, T., Luo, B. P., de Reus, M., Brunner, D., Cairo, F., Mahoney, M. J., et al. (2008). Unprecedented evidence for deep convection hydrating the tropical stratosphere. *Geophysical Research Letters*, *35*, L10810. https://doi.org/10.1029/2008GL033641

Davis, S. M., Rosenlof, K. H., Hassler, B., Hurst, D. F., Read, W. G., Vömel, H., et al. (2016). The Stratospheric Water and Ozone Satellite Homogenized (SWOOSH) database: A long-term database for climate studies. *Earth System Science Data*, *8*(2), 461–490. https://doi.org/10.5194/essd-8-461-2016

Dessler, A. E., Hanisco, T. F., & Fueglistaler, S. (2007). Effects of convective ice lofting on H_2O and HDO in the tropical tropopause layer. *Journal of Geophysical Research*, *112*, D18309. https://doi.org/10.1029/2007JD008609

Dessler, A. E., Schoeberl, M. R., Wang, T., Davis, S. M., & Rosenlof, K. H. (2013). Stratospheric water vapor feedback. *Proceedings of the National Academy of Science*, *110*(45), 18,087–18,091. https://doi.org/10.1073/pnas.1310344110

Forster, P. M. D., & Shine, K. P. (1999). Stratospheric water vapour changes as a possible contributor to observed stratospheric cooling. *Geophysical Research Letters*, *26*(21), 3309–3312. https://doi.org/10.1029/1999GL010487

Fueglistaler, S., Bonazzola, M., Haynes, P. H., & Peter, T. (2005). Stratospheric water vapor predicted from the Lagrangian temperature history of air entering the stratosphere in the tropics. *Journal of Geophysical Research*, *110*, D08107. https://doi.org/10.1029/2004JD005516

Fueglistaler, S., & Haynes, P. H. (2005). Control of interannual and longer-term variability of stratospheric water vapor. *Journal of Geophysical Research*, *110*, D24108. https://doi.org/10.1029/2005JD006019

Fueglistaler, S., Liu, Y. S., Flannaghan, T. J., Haynes, P. H., Dee, D. P., Read, W. J., et al. (2013). The relation between atmospheric humidity and temperature trends for stratospheric water. *Journal of Geophysical Research: Atmospheres*, *118*, 1052–1074. https://doi.org/10.1002/jgrd.50157

Fujiwara, M., Vömel, H., Hasebe, F., Shiotani, M., Ogino, S. Y., Iwasaki, S., et al. (2010). Seasonal to decadal variations of water vapor in the tropical lower stratosphere observed with balloon-borne cryogenic frost point hygrometers. *Journal of Geophysical Research*, *115*, D18304. https://doi.org/10.1029/2010JD014179

Garfinkel, C. I., Gordon, A., Oman, L. D., Li, F., Davis, S., & Pawson, S. (2018). Nonlinear response of tropical lower-stratospheric temperature and water vapor to ENSO. *Atmospheric Chemistry and Physics*, *18*(7), 4597–4615. https://doi.org/10.5194/acp-18-4597-2018

Geller, M. A., Zhou, X., & Zhang, M. (2002). Simulations of the interannual variability of stratospheric water vapor. *Journal of the Atmospheric Sciences*, *59*(6), 1076–1085. https://doi.org/10.1175/1520-0469(2002)059<1076:SOTIVO>2.0.CO;2

Gettelman, A., Kinnison, D. E., Dunkerton, T. J., & Brasseur, G. P. (2004). Impact of monsoon circulations on the upper troposphere and lower stratosphere. *Journal of Geophysical Research*, *109*, D22101. https://doi.org/10.1029/2004JD004878

Gilford, D. L., Solomon, S., & Portman, R. (2016). Radiative impacts of the 2011 abrupt drops in water vapor and ozone in the tropical tropopause layer. *Journal of Climate*, *29*(2), 595–612. https://doi.org/10.1175/JCLI-D-15-0167.1

Giorgetta, M. A., & Bengston, L. (1999). Potential role of the quasi-biennial oscillation in the stratosphere-troposphere exchange as found in water vapor in general circulation model experiments. *Journal of Geophysical Research*, *104*(D6), 6003–6019. https://doi.org/10.1029/1998JD200112

Glanville, A. A., & Birner, T. (2017). Role of vertical and horizontal mixing in the tape recorder signal near the tropical tropopause. *Atmospheric Chemistry and Physics*, *17*(6), 4337–4353. https://doi.org/10.5194/acp-17-4337-2017

Hanisco, T. F., Moyer, E. J., Weinstock, E. M., St. Clair, J. M., Sayres, D. S., Smith, J. B., et al. (2007). Observations of deep convective influence on stratospheric water vapor and its isotopic composition. *Geophysical Research Letters*, *34*, L04814. https://doi.org/10.1029/2006GL027899

Hegglin, M. I., Plummer, D. A., Shepherd, T. G., Scinocca, J. F., Anderson, J., Froidevaux, L., et al. (2014). Vertical structure of stratospheric water vapour trends derived from merged satellite data. *Nature Geoscience*, *7*(10), 768–776. https://doi.org/10.1038/NGEO2236

Hurst, D. F., Read, W. G., Vömel, H., Selkirk, H. B., Rosenlof, K. H., Davis, S. M., et al. (2016). Recent divergences in stratospheric water vapor measurements by frost point hygrometers and the Aura Microwave Limb Sounder. *Atmospheric Measurement Technologies*, *9*, 4447–4457. https://doi.org/10.5194/amt-9-4447-2016, www.atmos-meas-tech.net/9/4447/2016/

Jensen, E., & Pfister, L. (2004). Transport and freeze-drying in the tropical tropopause layer. *Journal of Geophysical Research*, *109*, D02207. https://doi.org/10.1029/2003JD004022

Kawatani, Y., Lee, J. N., & Hamilton, K. (2014). Interannual variations of stratospheric water vapor in MLS observations and climate model simulations. *Journal of the Atmospheric Sciences*, *71*(11), 4072–4085. https://doi.org/10.1175/JAS-D-14-0164.1

Khaykin, S., Pommereau, J. P., Korshunov, L., Yushkov, V., Nielsen, J., Larsen, N., et al. (2009). Hydration of the lower stratosphere by ice crystal geysers over land convective systems. *Atmospheric Chemistry and Physics*, *9*(6), 2275–2287. https://doi.org/10.5194/acp-9-2275-2009

Kim, J.-E., & Alexander, M. J. (2015). Direct impacts of waves on tropical cold point tropopause temperature. *Geophysical Research Letters*, *42*, 1584–1592. https://doi.org/10.1002/2014GL062737

Kley, D., Russell, J. M. III & Phillips, C. (Eds.) (2000). *SPARC Assessment of Upper Tropospheric and Stratospheric Water Vapour. WMO/ICSU/IOC World Climate Research Programme (WCRP)*. France.

Konopka, P., Ploeger, F., Tao, M. C., & Riese, M. (2016). Zonally resolved impact of ENSO on the stratospheric circulation and water vapor entry values. *Journal of Geophysical Research: Atmospheres*, *121*, 11,486–11,501. https://doi.org/10.1002/2015JD024698

Liang, C. K., Eldering, A., Gettelman, A., Tian, B., Wong, S., Fetzer, E. J., & Liou, K. N. (2011). Record of tropical interannual variability of temperature and water vapor from a combined AIRS-MLS data set. *Journal of Geophysical Research*, *116*, D06103. https://doi.org/10.1029/2010JD014841

Livesey, N. J., Read, W. G., Wagner, P. A., Froidevaux, L., Lambert, A., Manney, G. L., et al. (2018). Aura Microwave Limb Sounder (MLS) version 4.2x level 2 data quality and description document. Tech. Rep., Jet Propulsion Laboratory. Retrieved from http://mls.jpl.nasa.gov/

Maycock, A. C., Joshi, M. M., Shine, K. P., & Scaife, A. A. (2013). The circulation response to idealized changes in stratospheric water vapor. *Journal of Climate*, *26*(2), 545–561. https://doi.org/10.1175/JCLID-12-00155.1

Mote, P. W., Dunkerton, T. J., McIntyre, M. E., Ray, E. A., Haynes, P. H., & Russell, J. M. III (1998). Vertical velocity, vertical diffusion, and dilution by midlatitude air in the tropical lower stratosphere. *Journal of Geophysical Research*, *103*(D8), 8651–8666. https://doi.org/10.1029/98JD00203

Mote, P. W., Rosenlof, K. H., Holton, J. R., Harwood, R. S., & Waters, J. W. (1996). An atmospheric tape recorder: The imprint of tropical tropopause temperatures on stratospheric water vapor. *Journal of Geophysical Research*, *101*(D2), 3989–4006. https://doi.org/10.1029/95JD03422

Niwano, M., Yamazaki, K., & Shiotani, M. (2003). Seasonal and QBO variations in ascent rate in the tropical lower stratosphere as inferred from UARS HALOE trace gas data. *Journal of Geophysical Research*, *108*(D24), 4794. https://doi.org/10.1029/2003JD003871

Nützel, M., Podglajen, A., Garny, H., & Ploeger, F. (2019). Quantification of water vapour transport from the Asian monsoon to the stratosphere. *Atmospheric Chemistry and Physics Discussions*, 1–32. https://doi.org/10.5194/acp-2019-169

Ploeger, F., & Birner, T. (2016). Seasonal and inter-annual variability of lower stratospheric age of air spectra. *Atmospheric Chemistry and Physics*, *16*(15), 10195–10213. https://doi.org/10.5194/acp-16-10195-2016

Poshyvailo, L., Müller, R., Konopka, P., Günther, G., Riese, M., Podglajen, A., & Ploeger, F. (2018). Sensitivities of modelled water vapour in the lower stratosphere: Temperature uncertainty, effects of horizontal transport and small-scale mixing. *Atmospheric Chemistry and Physics*, *18*(12), 8505–8527. https://doi.org/10.5194/acp-18-8505-2018

Randel, W. J. (2010). Variability and trends in stratospheric temperature and water vapor. In L. M. Polvani, A. H. Sobel, & W. Waugh (Eds.), *The stratosphere: Dynamics, transport and chemistry*, *Geophys. Monogr. Ser.* (Vol. 190, pp. 123–135). Washington, DC: American Geophysical Union. https://doi.org/10.1029/2009GM000870

Randel, W. J., & Jensen, E. (2013). Physical processes in the tropical tropopause layer and their role in a changing climate. *Nature Geoscience*, *6*(3), 169–176. https://doi.org/10.1038/ngeo1733

Randel, W. J., Wu, F., Gettelman, A., Russell, J. M. III, Zawodny, J. M., & Oltmans, S. J. (2001). Seasonal variation of water vapor in the lower stratosphere observed in Halogen Occultation Experiment data. *Journal of Geophysical Research*, *106*(D13), 14,313–14,325. https://doi.org/10.1029/2001JD900048

Randel, W. J., Wu, F., Oltmans, S., Rosenlof, K., & Nedoluha, G. (2004). Interannual changes of stratospheric water vapor and correlations with tropical tropopause temperatures. *Journal of the Atmospheric Sciences*, *61*(17), 2133–2148. https://doi.org/10.1175/1520-0469(2004)061<2133:ICOSWV>2.0.CO;2

Randel, W. J., Wu, F., Russell, J. M. III, Roche, A., & Waters, J. (1998). Seasonal cycles and QBO variations in stratospheric CH_4 and H_2O observed in UARS HALOE data. *Journal of the Atmospheric Sciences*, *55*(2), 163–185. https://doi.org/10.1175/1520-0469(1998)055<0163:SCAQVI>2.0.CO;2

Randel, W. J., Zhang, K., & Fu, R. (2015). What controls stratospheric water vapor in the NH summer monsoon regions? *Journal of Geophysical Research: Atmospheres*, *120*, 7988–8001. https://doi.org/10.1002/2015JD023622

Read, W. G., Lambert, A., Bacmeister, J., Cofield, R. E., Christensen, L. E., Cuddy, D. T., et al. (2007). Aura Microwave Limb Sounder upper tropospheric and lower stratospheric H_2O and relative humidity with respect to ice validation. *Journal of Geophysical Research*, *112*, D24S35. https://doi.org/10.1029/2007JD008752

Remsberg, E. E., Bhatt, P. P., & Russell, J. M. III (1996). Estimates of the water vapor budget of the stratosphere from UARS HALOE data. *Journal of Geophysical Research*, *101*(D3), 6749–6766. https://doi.org/10.1029/95JD03858

Rosenlof, K. H., Tuck, A. F., Kelly, K. K., Russell, J. M. III, & McCormick, M. P. (1997). Hemispheric asymmetries in water vapor and inferences about transport in the lower stratosphere. *Journal of Geophysical Research*, *102*(D11), 13,213–13,234. https://doi.org/10.1029/97JD00873

Russell, J. M. III, Gordley, L. L., Park, J. H., Drayson, S. R., Hesketh, W. D., Cicerone, R. J., et al. (1993). The Halogen Occultation Experiment. *Journal of Geophysical Research*, *98*(D6), 10,777–10,797. https://doi.org/10.1029/93JD00799

Schiller, C., Grooß, J. U., Konopka, P., Ploger, F., Silva dos Santos, F. H., & Spelten, N. (2009). Hydration and dehydration at the tropical tropopause. *Atmospheric Chemistry and Physics*, *9*(24), 9647–9660. www.atmos-chem-phys.net/9/9647/2009/, https://doi.org/10.5194/acp-9-9647-2009

Schoeberl, M., Dessler, A., Ye, H., Wang, T., Avery, M., & Jensen, E. (2016). The impact of gravity waves and cloud nucleation threshold on stratospheric water and tropical tropospheric cloud fraction. *Earth and Space Science*, *3*, 295–305. https://doi.org/10.1002/2016EA000180

Schoeberl, M., Jensen, E. J., Pfister, L., Ueyama, R., Avery, M., & Dessler, A. E. (2018). Convective hydration of the upper troposphere and lower stratosphere. *Journal of Geophysical Research: Atmospheres*, *123*, 4583–4593. https://doi.org/10.1029/2018JD028286

Schoeberl, M. R., & Dessler, A. E. (2011). Dehydration of the stratosphere. *Atmospheric Chemistry and Physics*, *11*(16), 8433–8446. https://doi.org/10.5194/acp-11-8433-2011

Schoeberl, M. R., Dessler, A. E., & Wang, T. (2012). Simulation of stratospheric water vapor and trends using three reanalyses. *Atmospheric Chemistry and Physics*, *12*(14), 6475–6487. https://doi.org/10.5194/acp-12-6475-2012

Schoeberl, M. R., Douglass, A. R., Stolarski, R. S., Pawson, S., Strahan, S. E., & Read, W. (2008). Comparison of lower stratospheric tropical mean vertical velocities. *Journal of Geophysical Research*, *113*, D24109. https://doi.org/10.1029/2008JD010221

Solomon, S., Rosenlof, K. H., Portmann, R. W., Daniel, J. S., Davis, S. M., Sanford, T. J., & Plattner, G. K. (2010). Contributions of stratospheric water vapor to decadal changes in the rate of global warming. *Science*, *327*(5970), 1219–1223. https://doi.org/10.1126/science.1182488

Sun, Y., & Huang, Y. (2015). An examination of convective moistening of the lower stratosphere using satellite data. *Earth and Space Science*, *2*, 320–330. https://doi.org/10.1002/2015EA000115

Tao, M., Konopka, P., Ploeger, F., Riese, M., Müller, R., & Volk, C. M. (2015). Impact of stratospheric major warmings and the quasi-biennial oscillation on the variability of stratospheric water vapor. *Geophysical Research Letters*, *42*, 4599–4607. https://doi.org/10.1002/2015GL064443

Tweedy, O. V., Kramarova, N. A., Strahan, S. E., Newman, P. A., Coy, L., Randel, W. J., et al. (2017). Response of trace gases to the disrupted 2015–2016 quasi-biennial oscillation. *Atmospheric Chemistry and Physics*, *17*(11), 6813–6823. https://doi.org/10.5194/acp-17-6813-2017

Ueyama, R., Jensen, E. J., & Pfister, L. (2018). Convective influence on the humidity and clouds in the tropical tropopause layer during boreal summer. *Journal of Geophysical Research: Atmospheres*, *123*, 7576–7593. https://doi.org/10.1029/2018JD028674

Ueyama, R., Jensen, E. J., Pfister, L., & Kim, J.-E. (2015). Dynamical, convective, and microphysical control on wintertime distributions of water vapor and clouds in the tropical tropopause layer. *Journal of Geophysical Research: Atmospheres*, *120*, 10,483–10,500. https://doi.org/10.1002/2015JD023318

Wang, T., Dessler, A. E., Schoeberl, M. R., Randel, W. J., & Kim, J. E. (2015). The impact of temperature vertical structure on trajectory modeling of stratospheric water vapor. *Atmospheric Chemistry and Physics*, *15*(6), 3517–3526. https://doi.org/10.5194/acp-15-3517-2015

Waugh, D. W., & Hall, T. M. (2002). Age of stratospheric air: Theory, observations, and models. *Reviews of Geophysics*, *40*(4), 1010. https://doi.org/10.1029/2000RG000101